FEATURE ARTICLE

Amplification and attenuation of increased primary production in a marine food web

Kelly A. Kearney[1,4,*], Charles Stock[2], Jorge L. Sarmiento[3]

[1]Department of Geosciences, Princeton University, Princeton, New Jersey 08544, USA

[2]Geophysical Fluid Dynamics Laboratory (GFDL), National Oceanic and Atmospheric Administration (NOAA), 201 Forrestal Road, Princeton, New Jersey 08540, USA

[3]Program in Atmospheric and Ocean Sciences, Princeton University, Princeton, New Jersey 08544, USA

[4]*Present address:* Marine Biology and Fisheries, University of Miami Rosenstiel School of Marine and Atmospheric Sciences, 4600 Rickenbacker Causeway, Miami, Florida 33149, USA

ABSTRACT: We used an end-to-end ecosystem model that incorporates physics, biogeochemistry, and predator–prey dynamics for the Eastern Subarctic Pacific ecosystem to investigate the factors controlling propagation of changes in primary production to higher trophic levels. We found that lower trophic levels respond to increased primary production in unexpected ways due to complex predatory interactions, with small phytoplankton increasing more than large phytoplankton due to relief from predation by microzooplankton, which are kept in check by the more abundant mesozooplankton. We also found that the propagation of production to upper trophic levels depends critically on how non-predatory mortality is structured in the model, with much greater propagation occurring with linear mortality and much less with quadratic mortality, both of which functional forms are in common use in ecosystem models. We used an ensemble simulation approach to examine how uncertainties in model parameters affect these results. When considering the full range of potential responses to enhanced productivity, the effect of uncertainties related to the functional form of non-predatory mortality was often masked by uncertainties in the food-web parameterization. The predicted responses of several commercially important species, however, were significantly altered by non-predatory mortality assumptions.

KEY WORDS: End-to-end model · Trophic efficiency · Primary production · Food web · Subarctic Pacific Ocean · Ecosystem model
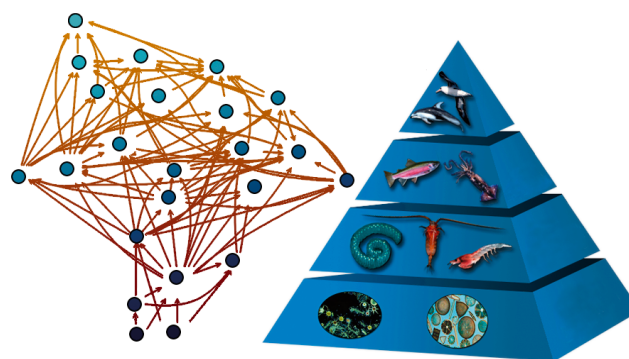
Realistic, complex marine food webs (left) complicate the simple paradigm of linear production and energy transfer across trophic levels (right).

Image: Eileen Kearney

INTRODUCTION

How closely linked to net primary production is the production of upper-trophic-level consumers? Classical food chain theory suggests that a constant fraction of production (approximately 10 %) is transferred from each trophic level to the next (Pauly & Christensen 1995, May & McLean 2007), and a variety of regional studies have shown positive linear trends between common indicators of primary production (such as chlorophyll *a*) and fisheries yields (Ware et al. 2005, Frank et al. 2006, Chassot et al. 2007). However, in their analysis of bottom-up predictor variables versus fisheries yields, Friedland et al. (2012)

*Email: kkearney@rsmas.miami.edu

found that phytoplankton production itself was a very poor predictor of fisheries yields over globally distributed systems. Across ecosystems, they found that metrics that accounted for variations in trophic transfer efficiency and the size structure of the planktonic food web, such as the particle export ratio or the mesozooplankton to primary production ratio, were more highly correlated with fisheries yields than primary production. The variation in the relationship between primary production and fisheries production across different ocean environments is in keeping with classical studies, which estimated very different transfer efficiencies in marine food webs under varying environmental conditions (coastal versus open ocean versus upwelling areas) (Ryther 1969). Improved understanding of fisheries yields and fisheries capacity requires refinements beyond an estimated 10% transfer efficiency between trophic levels (e.g. Pauly & Christensen 1995).

A nearly universal characteristic of marine ecosystem models is the inclusion of 'non-predatory loss terms'. These terms are used to represent the net effect of a diversity of loss processes, including natural mortality (i.e. death due to old age), loss to disease and viruses, unresolved intra-group mortality (such as egg cannibalism and predation on juveniles of similar species), aggregation and sinking out of the modeled system (primarily of large phytoplankton), and respiration. As these terms channel energy away from higher predators, choices concerning the size and functional form of these terms also have the potential to influence the flow of energy to higher trophic levels. Historically, fisheries ecosystem models, such as Ecopath with Ecosim, tend to assume a linear relationship between biomass of a functional group and loss due to non-predatory processes (Christensen & Walters 2004). However, plankton models tend to use quadratic mortality closures to achieve stability and match observed seasonal cycles (Steele & Henderson 1992, Edwards & Yool 2000). Both functional forms can be appropriate for different contributing processes of the non-predatory loss; viral loss (Brussaard 2004), intra-group predation mortality (Ohman & Hirche 2001), and aggregation (Thornton 2002) are often observed to be density-dependent processes, and may be better modeled by a quadratic form, whereas basal metabolic rate is generally assumed to be constant per unit biomass and thus would be better modeled with a linear formula (Flynn 2005).

The structural uncertainties presented by uncertain process formulations, such as that of non-predatory mortality, are further complicated by the already high parameter uncertainty that exists in complex ecosystem models. Population-scale variables, such as standing stock biomass, are challenging to compile for an entire ecosystem. The large range in spatial scales covered by these ecosystems makes it very difficult to thoroughly survey the population of even a single target fish species, for which there may be regular scientific sampling programs as well as plentiful fisheries-based observations. Non-target species, such as myctophids or other forage fish, play equally key roles in ecosystem dynamics as fisheries-targeted species, but there is far less data available regarding the populations of these species. Seabirds are often counted only at their roosting spots, but forage over a much larger swath of ocean, while whales may migrate thousands of miles to forage. Gelatinous zooplankton may play important roles in mesozooplankton communities, but are inadequately sampled by traditional net tows; therefore there is far less data on them than their crustacean counterparts. The lack of plentiful observations at all levels of the food web can lead to wide error bars on the input parameters used in ecosystem models, and this uncertainty is propagated to the output of any simulations.

In this study, we attempted to quantify and understand the factors controlling the response of the end-to-end ecosystem model to a bottom-up perturbation, namely an increase in net primary production due to alleviation of micronutrient limitation. The impact of non-predatory mortality on the energy flow through the system was quantified and drivers of the amplification of primary productivity perturbations were diagnosed. We also assessed the contribution of uncertainties in non-predatory loss structure to the overall uncertainty of the upper-trophic-level productivity response to primary production changes.

METHODS

Description of the ecosystem model

We used an end-to-end ecosystem model that fully couples physics, biogeochemistry, and predator–prey dynamics for the Eastern Subarctic Pacific ecosystem (Kearney et al. 2012). The physical portion of this model simulated the seasonal evolution of a one-dimensional water column, resolved vertically and forced at the surface by winds, radiation, and temperature. The biogeochemical and food-web portion of the model was coupled to the physical model, and tracked state variables that encompass the nutrient cycles of nitrogen, silicon, and iron, as well as the

primary production and predator–prey interactions between 2 phytoplankton (P) functional groups, 5 zooplankton (Z) functional groups, and 16 'nekton' (i.e. non-planktonic organisms, including fish, squid, mammals, and birds) (K) functional groups (Figs. 1 & 2, Table 1). The distinction between plankton and nekton indicates how each group is coupled to the physical model; planktonic groups are resolved vertically, subject to physical mixing, and feed only on prey within the same grid cell, whereas nektonic groups are not vertically resolved and view prey fields as the integrated sum over the water column.

All components of the model, including physical interactions, biogeochemical cycling, and predator–prey dynamics, were calculated in a fully coupled manner at each time step, with 2-way feedback throughout the entire food web. For a complete description of the model, including both physical and biological components, as well as description of all parameters used for this study, see the Supplement at www.int-res.com/articles/suppl/m491p001_supp.pdf.

The food-web portion of the model represents the Eastern Subarctic Gyre of the North Pacific, which is an important foraging ground for a variety of epipelagic species (Brodeur et al. 1999), and a rearing and growth area for commercially important Pacific salmon (Aydin et al. 2005). Although the model was parameterized for this specific region, the processes included are generic across open ocean ecosystems, and the analysis in this paper is intended as a more general exploration applicable to all models of similar type. This sensitivity study looked specifically at the changes that arise through direct propagation of net primary productivity through the food web, isolating this from any direct effects of climate on upper-trophic-level groups.

The Eastern Subarctic Pacific Gyre region is a high-nutrient, low-chlorophyll region, with iron playing the role of limiting nutrient (Martin & Fitzwater 1988, Martin et al. 1989). Therefore, the easiest way to systematically augment primary production in this model was to alleviate the iron limitation through increased surface deposition of iron. Note that in designing this experiment, we were not attempting to replicate a short-term iron-fertilization experiment, but rather to look at the

Fig. 1. The food web used for this study incorporates 23 living functional groups. The predator–prey interactions between these groups are shown here, with arrows pointing from prey to predator. The axis to the left indicates the trophic level of each group, following the Ecopath definition where trophic level of a consumer is equal to 1 plus the diet-fraction-weighted average of its prey's trophic levels. See Table 1 for identification and description of each functional group
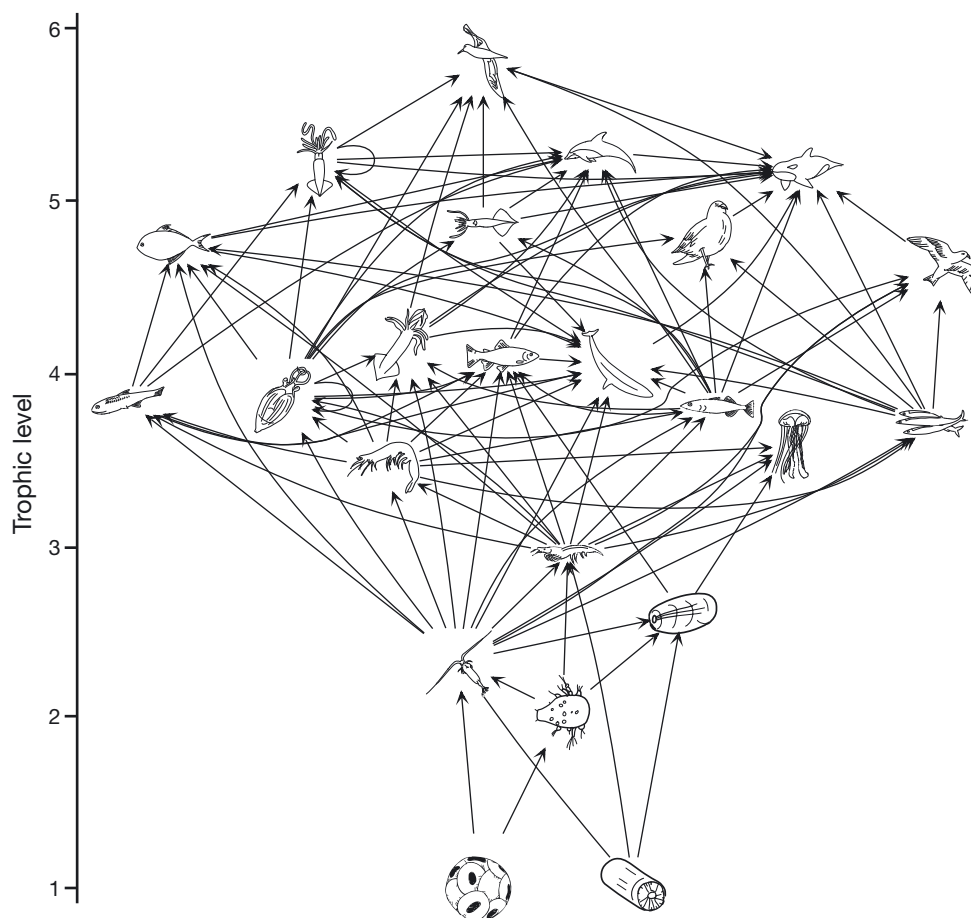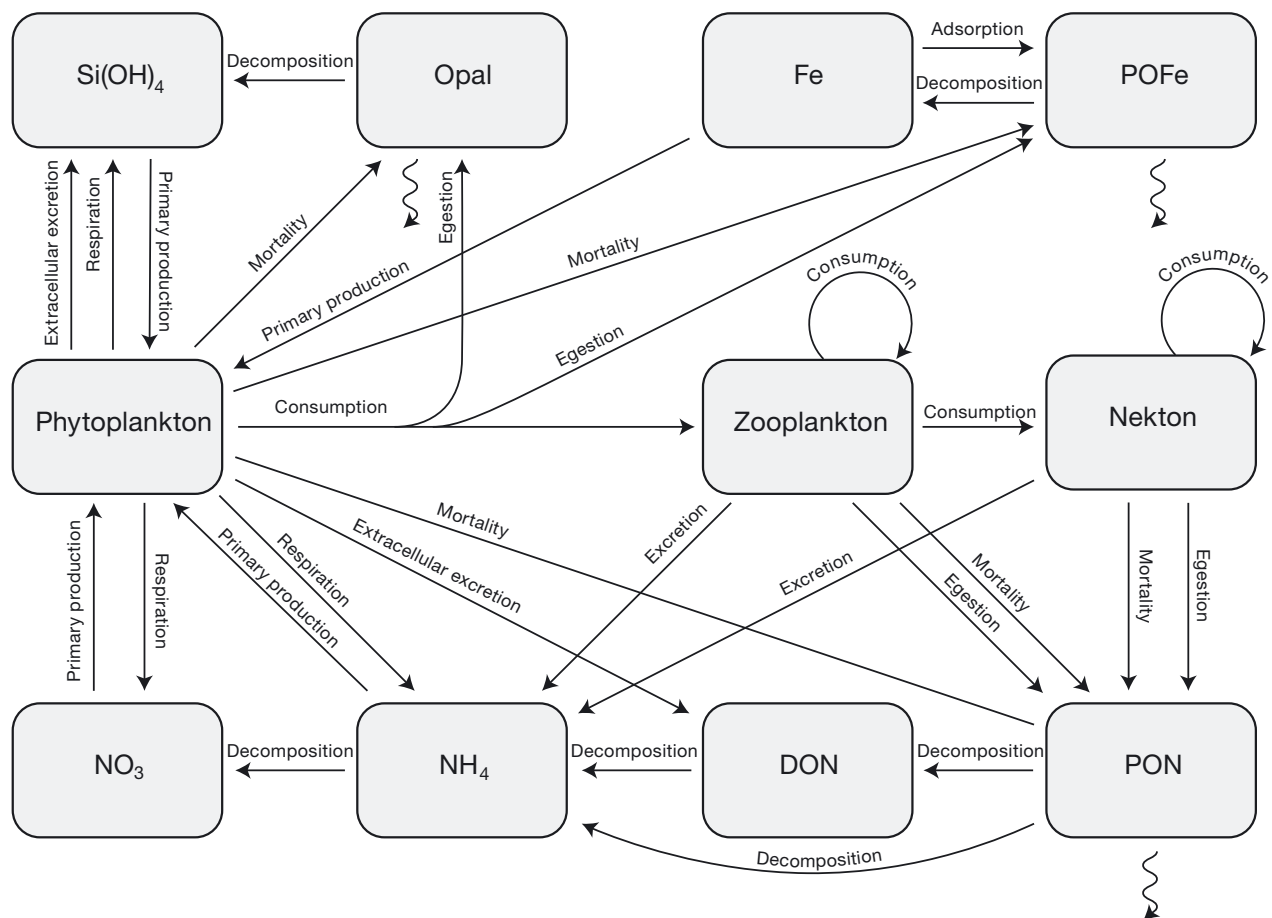
Fig. 2. Water column ecosystem model processes and state variables. The phytoplankton, zooplankton, and nekton boxes represent classes of variables; Fig. 1 diagrams the connections between each of the individual functional groups state variables represented by these classes. Wavy arrows indicate state variables that sink in the model. Fe: dissolved iron; POFe: particulate iron; DON: dissolved organic nitrogen; PON: particulate organic nitrogen

response of the entire ecosystem to a long-term change in productivity, such as those due to persistent shifts in iron dust sources or atmospheric transport (Luo et al. 2008, Mahowald et al. 2009) or other projected effects of climate change (Steinacher et al. 2010)

As iron plays a central role in this set of simulations, we implemented an improved representation of iron dynamics following Stock et al. (in press). Rather than the relaxation scheme used in Kearney et al. (2012), we explicitly resolved 2 forms of iron: dissolved iron and particulate iron (Fig. 2). The iron model uses a single ligand to bind free iron (Johnson et al. 1997), with free iron scavenged onto sinking detritus at a constant linear rate. Iron binding becomes less effective in well-lit areas due to photochemical effects (Fan 2008). While this representation of iron-scavenging dynamics is simple relative to the full scope of iron chemistry and particle interac-

tions (Boyd & Ellwood 2010), we emphasize that the primary objective of this contribution was to understand the response of an end-to-end model to perturbations in primary productivity. Climatological surface iron deposition was derived from the Geophysical Fluid Dynamics Laboratory Global Chemical Transport model's soluble iron flux, extracted at the location of Ocean Station Papa (50° N, 145° W) (Moxim et al. 2011).

Simulation setup

To quantify the propagation of increased primary production to higher trophic levels in the context of model uncertainty, we ran several sets of simulations, varying the strength of the perturbation, the functional form of non-predatory mortality loss, and the model parameterization.

Table 1. The simplified food-web model includes 23 functional groups, listed below along with the picture used to identify each in the food-web diagram (Fig. 1). The type column indicates whether each group is classified as phytoplankton (P), zooplankton (Z), or nekton (K) in the fully coupled model. See the Supplement (www.int-res.com/articles/suppl/m491p001_supp.pdf) for a more complete description of each group

Index	Name	Type	Symbol	Consolidated groups
1	Albatross	K		Albatross
2	Mammals and sharks	K		Northern elephant seals, northern fur seals, sperm whales, Dall's porpoises, Pacific white sided dolphins, northern right whale dolphins, sharks
3	Neon flying squid	K		Neon flying squid
4	Orcas	K		Toothed whales
5	Boreal clubhook squid	K		Boreal clubhook squid
6	Seabirds 1	K		Skuas, jaegars, fulmars
7	Pomfret	K		Pomfret
8	Seabirds 2	K		Shearwaters, storm petrels, kittiwakes, puffins
8	Large gonatid squid	K		Large gonatid squid
10	Salmon	K		Coho salmon, pink salmon, sockeye salmon, chum salmon, Chinook salmon, steelhead
11	Baleen whales	K		Fin whales, sei whales
12	Micronektonic squid	K		Micronektonic squid
13	Mesopelagic fish	K		Mesopelagic fish
14	Pelagic forage fish	K		Pelagic forage fish
15	Saury	K		Saury
16	Large jellyfish	K		Jellyfish
17	Predatory zooplankton	Z		Sergestid shrimp, chaetognaths, miscellaneous predatory zooplankton
18	Large zooplankton	Z		Euphausiids, amphipods, pteropods
19	Gelatinous zooplankton	Z		Salps, ctenophores
20	Copepods	Z		Copepods
21	Microzooplankton	Z		Microzooplankton
22	Small phytoplankton	P		Small phytoplankton
23	Large phytoplankton	P		Large phytoplankton

Each simulation consisted of a 10 yr climatological spin-up period, followed by a 10 yr increased iron-deposition period. We systematically raised the surface deposition flux of iron from its climatological annually averaged value of 2.83 pmol Fe m^{-2} s^{-1} to values 1.25, 1.5, 2.0, 3.0, and 5.0 times higher than that. The 1.25× perturbation captures the approximate magnitude of interannual variability in dust deposition in the subarctic gyre, while the higher values represent levels that might be expected more rarely, such as in response to volcanic activity in the nearby Aleutian Islands (Duggen et al. 2007), or perhaps from a long-term increase in combustion-related sources (Luo et al. 2008). For our quantitative analysis, we used values from the final year of each simulation. While not every functional group had reached a completely new steady state by the 10 and 20 yr marks, all groups showed less than 1.5% change in yearly averaged biomass per year at the end of the climatological period and even the slowest-growing groups showed less than a 5% change 10 yr after the strongest perturbations; therefore, we felt this spin-up time was sufficient for our analyses.

The biogeochemical and food-web portion of the model incorporates observational uncertainty into the parameters constraining predator–prey functional response, non-predatory mortality, and initial biomass through the use of an intramodel ensemble. The ensemble is derived though the use of Ecopath models (Christensen & Pauly 1992); the biomass, production/biomass, consumption/biomass, and diet composition variables assigned to each functional group are associated with an uncertainty range based on the quality of data from which they are derived, and parameter sets are then chosen from log-normal distributions defined by these parameters, filtered such that all parameter sets used meet the mass-balance criteria of the Ecopath algorithm (Aydin et al.

2007, Kearney 2012). The same set of 50 ensemble members was run for each combination of surface iron flux and mortality formulation. See the Supplement for the parameter values associated with the ensemble members. To assess the impact of the assumed form of non-predatory mortality, all consumer groups were run with non-predatory mortality functions of the form:

$$M_0 = aB^c \qquad (1)$$

where M_0 is the total loss due to non-predatory mortality (mol N m^{-3} s^{-1} for plankton, mol N m^{-2} s^{-1} for nekton), B is the biomass of the group (mol N m^{-3} for plankton, mol N m^{-2} for nekton), and c was set to either 1.0, 1.5, or 2.0, representing linear, mixed, and quadratic mortality, respectively. The coefficient a was constrained through the Ecopath-derived values for biomass (B^*, the mass-balanced biomass of a functional group) and M_0^* (the mass-balanced value for all group production not passed to higher trophic levels) such that $a = M_0^*/(B^{*c})$. The quadratic structure captures the end case where density-dependent processes are the primary contributors to non-predatory loss, whereas the linear structure represents the other end case where density-independent processes predominate. Note that producer groups used a quadratic non-predatory mortality term in all scenarios; this form was necessary to maintain proper seasonal dynamics in primary production, as discussed in Kearney et al. (2012). We encountered some issues when attempting to analyze the results of the purely linear mortality case. While we wanted to include this formulation as a critical end case representing non-density dependent processes, the linear case is mathematically less stable than higher-order functions (Armstrong 1999). Coupled with the high temporal resolution of the physical forcings included in this model, the instability manifests itself by causing some ensemble members to drift away from observed values, even under climatological conditions. To ensure consistent comparisons across all 3 mortality regimes, for our final analysis we considered only those ensemble members whose yearly averaged biomass values remained within the initial uncertainty ranges defined by the Ecopath model over all 3 mortality regimes, for a total of 39 ensemble members. In summary, 750 model simulations were run: 5 nutrient scenarios, 3 mortality scenarios, and 50 parameterization ensemble members; 585 (5 nutrient, 3 mortality, 39 ensemble) of these were used in the final analysis.

Simulation analysis

We calculated a variety of metrics to quantify the propagation of primary production through the ecosystem as a whole.

Total net primary production (NPP) was calculated as the sum of net primary production across both phytoplankton groups. We also calculated net secondary production (NSP) for each of the 21 consumer groups in the ecosystem.

To quantify the different patterns of propagation throughout the food web (and across the many orders of magnitude spanned by production rates from producers to top consumers), we defined a metric to relate relative change in net primary productivity (NPP$_{rel}$) to relative change in consumer productivity (NSP$_{rel}$), which we termed amplification. The amplification values were calculated by fitting a line to relative net total primary production versus relative net secondary production across all iron regimes, where relative values were defined as follows:

$$NPP_{rel} = \frac{NPP_{hiFe}}{NPP_{clim}} \qquad (2)$$

$$NSP_{rel,i} = \frac{NSP_{hiFe,i}}{NSP_{clim,i}} \qquad (3)$$

The slope of the fitted line across the 6 iron regimes (5 high-iron periods (hiFe) plus the climatological (clim) period) is defined as the amplification value, with one amplification value calculated per ensemble member, mortality regime, and functional group (i). While the trend across iron regimes was not always perfectly linear, 98% of the ensemble–mortality–group sets showed a significant fit to the linear regression ($p < 0.05$), and less than 5% of the fits had R^2 values of less than 0.9. An amplification value (NSP$_{rel}$/NPP$_{rel}$) of 1 indicates that a functional group's production remained the same proportional to the relative change in net primary production. A value greater than 1 indicates an amplification of the primary production signal, while a value less than 1 indicates an attenuation (the choice to refer to the metric as amplification rather than attenuation in the text of this paper was arbitrary).

We performed several regression analyses to elucidate the factors contributing to the differences in amplification between mortality regimes for a given ensemble member. The ratio of quadratic:linear amplification metric was regressed against trophic level and ecotrophic efficiency (i.e. fraction of mass-balanced loss attributed to predatory loss rather than non-predatory loss). We also performed a

multiple linear regression (with interaction terms) against the 2 predictors. Finally, we assessed the importance of assumptions concerning the functional form of non-predatory mortality relative to uncertainties in the food-web parameterization in determining the range of simulated responses to the primary production increase. To do this, we tested whether the differences between mortality regimes remained important when the ensemble members were treated as independent observations. For this comparison, we performed a Mann-Whitney U-test ($\alpha = 0.05$) to test whether the sample medians were significantly different between the linear and quadratic mortality regimes. We applied the test to both biomass and net secondary production for each functional group.

RESULTS

Primary productivity under enhanced iron deposition

Increased iron deposition led to an increase in total net primary productivity, although there was considerable variability in the magnitude of this increase across ensemble members, particularly at very high iron levels (Fig. 3). The increase in surface iron concentrations was approximately linear as surface deposition increased. In response, annually averaged net productivity increased until surface dissolved iron levels reached ~0.2 nM Fe, which occurs in the 3.0 deposition regime; beyond this level, macronutrients became limiting once more and primary production leveled off.
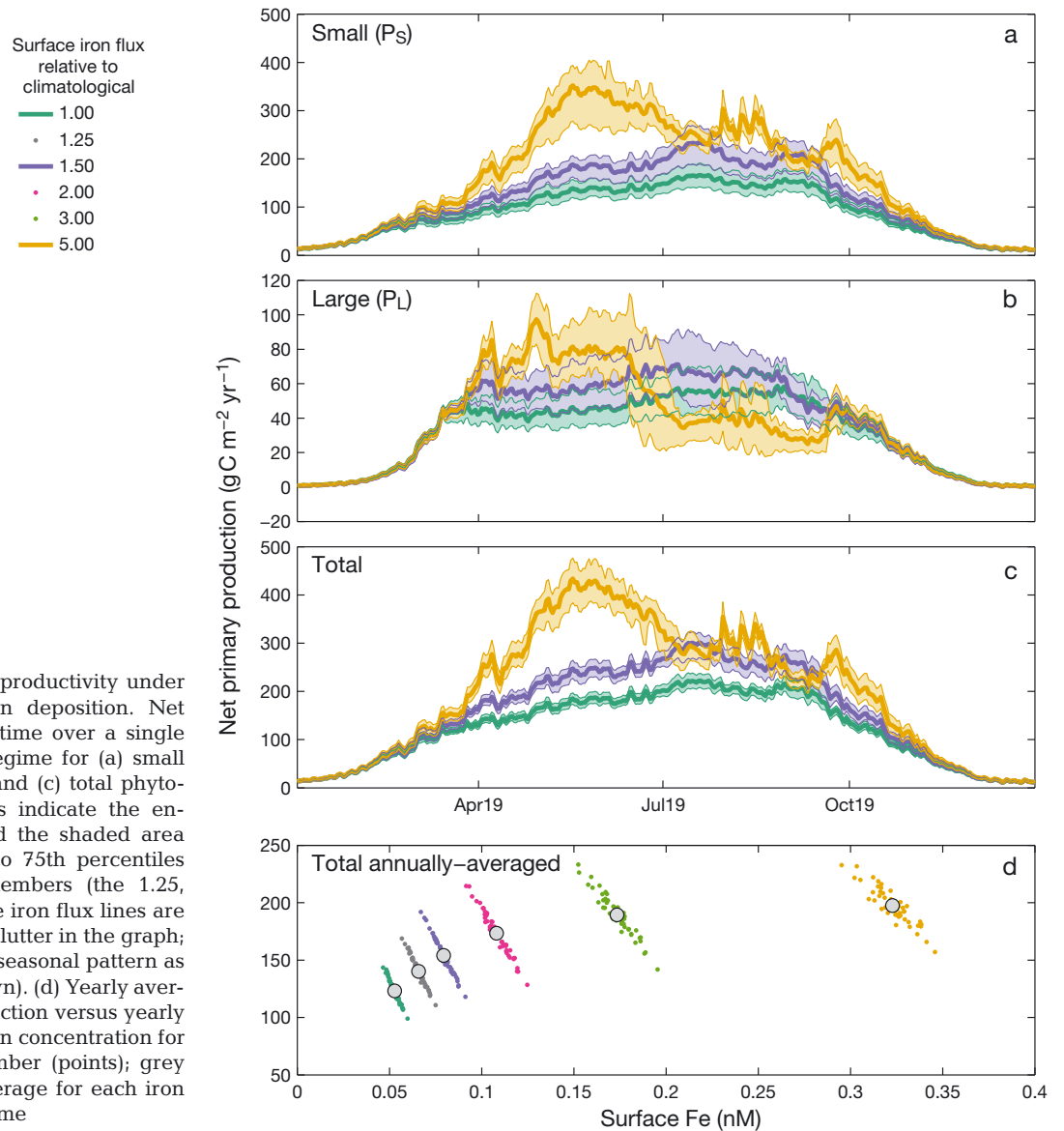
Fig. 3. Net primary productivity under varying surface iron deposition. Net productivity versus time over a single year of each iron regime for (a) small (P_S), (b) large (P_L), and (c) total phytoplankton. Bold lines indicate the ensemble average and the shaded area indicates the 25th to 75th percentiles across ensemble members (the 1.25, 2.0, and 3.0× surface iron flux lines are not shown to avoid clutter in the graph; they show a similar seasonal pattern as the simulations shown). (d) Yearly averaged total net production versus yearly averaged surface iron concentration for each ensemble member (points); grey circle: ensemble average for each iron regime

The increased primary productivity manifested itself primarily through increases in the small phytoplankton group. Large phytoplankton exhibited higher production in the spring, but decreased production in the fall under high iron deposition, which led to the annually averaged production values for this group remaining more or less constant across all 5 iron regimes. These responses were due to a combination of both bottom-up and top-down controls on the population growth of the larger size class. Enhanced iron deposition increased production by both size classes in the spring, when macronutrients are plentiful (Fig. 4). However, the enhanced bloom and high iron deposition early in the summer led to a depletion of macronutrients and an enhanced mesozooplankton community in late summer and early fall, both of which strongly limit the production of the large phytoplankton population. The newly strengthened mesozooplankton community maintained a strong top-down control on the microzooplankton group, which is the primary predator of small phytoplankton, allowing small phytoplankton biomass and production to expand. Although observations of the North Pacific phytoplankton community response to a long-term change like the one we simulated are not available to either confirm or refute our results, the increased net primary production levels under the higher surface iron flux conditions allowed us to closely analyze the propagation of production to

higher trophic levels. We will revisit the simulated response to iron enrichment in the 'Discussion' section.

Propagation of productivity to higher trophic levels

In our simulation results, increased net primary production led to increased consumer net secondary production for all functional groups included in this model (Fig. 5). However, the sensitivity of consumer production to changes in net primary production varied widely across both ensemble members and mortality structures. We saw smaller absolute changes in consumer production at higher trophic levels, but this was primarily a reflection of the overall decline in energy flows as one moves to higher trophic levels.

Analysis of relative changes in production through the amplification metric (Eqs. 2 & 3) revealed differences in the response of the food web under the 3 different mortality structures (Fig. 6). At the lowest trophic levels, the microzooplankton and copepod groups showed no significant difference in amplification between the linear and quadratic mortality schemes. For all 3 sets of simulations, the change in microzooplankton production was amplified relative to primary production, while the change in copepod production was attenuated, indicating a shift in the food web towards the smaller size class. This was consistent with the simulated redistribution of primary production (Fig. 3). While stronger top-down control restricted the biomass of small zooplankton, the subsequent enhancement of small phytoplankton production increased the overall energy flow through small zooplankton.

The remaining functional groups did see a significant difference in the amplification metric across mortality schemes. Under the quadratic scheme, all groups except the microzooplankton showed median values less than 1, indicating that a higher fraction of ecosystem production was being lost to non-predatory loss terms under high-production conditions than under low-production conditions. On the other hand, under the linear mortality scheme, the majority of the groups had median amplification values greater than 1, indicating that more production is staying within the food web and being passed to higher trophic levels, rather than being lost to non-predatory sources. Our regression analysis revealed that both
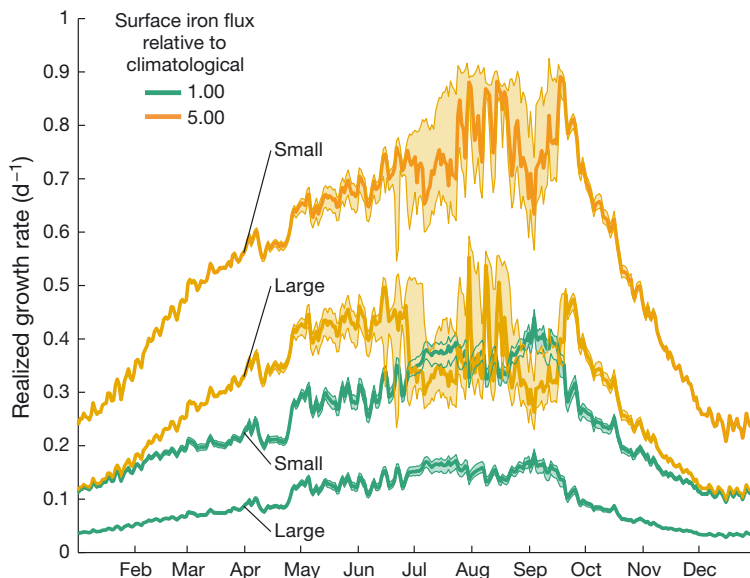

Fig. 4. Realized growth rates (i.e. light- and nutrient-limited growth rates) for large and small phytoplankton under climatological (1.0×) and 5.0× surface iron deposition levels. The realized growth rates for both functional groups increase under the high-iron conditions. Shaded areas represent the 25 to 75% ensemble range and the solid lines indicate the ensemble median
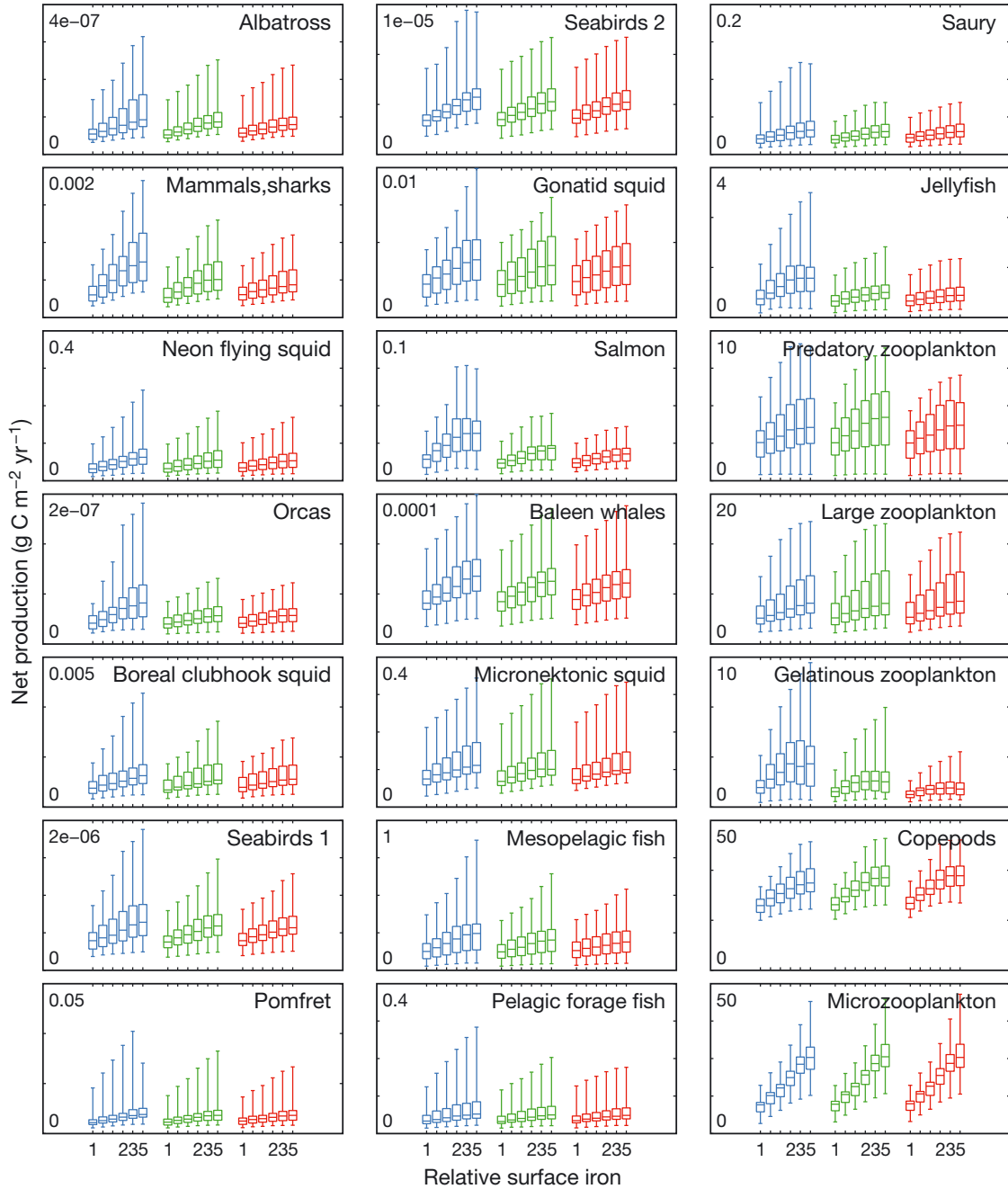
Fig. 5. Net consumer secondary production across all simulations. The *x*-axis coordinates indicate the simulated surface iron deposition relative to climatological levels, for linear (blue), mixed (green), and quadratic (red) mortality schemes, and the *y*-axis indicates the annually averaged net consumer production

trophic level and ecotrophic efficiency showed statistically significant relationships with the relative amplification between the linear and quadratic regimes (Table 2).

Higher trophic levels tended to show larger difference between the 2 mortality regimes, as did functional groups with larger mass-balanced non-predatory loss fractions (i.e. lower ecotrophic efficiencies).

However, together these 2 factors only explained a modest amount of the overall variability, illustrating the complex dependence of individual functional group responses on food-web interactions, including the responses of preferred prey, competitors, and primary predators.

Across the entire ensemble of projected responses, differences in the simulated response to enhanced
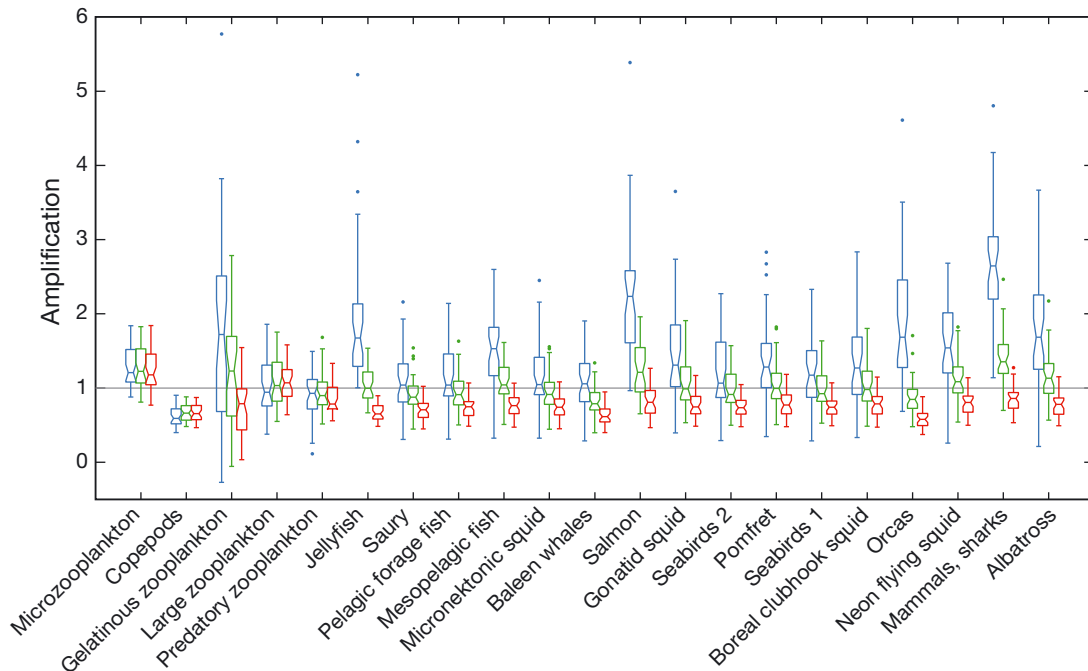
Fig. 6. Amplification metric across all simulations. The amplification metric quantifies the strengthening or weakening of a change in production across trophic levels. These boxplots show the spread of values for each consumer; boxes indicate 25th to 75th percentiles across ensemble members, with a central mark at the median, whiskers extend to the maximum and minimum non-outlier values, and outliers are marked as points. Two medians are significantly different (at the 5 % level) if their notch ranges (i.e. region from bottom narrowing point to top narrowing point) do not overlap. As in Fig. 5, blue, green, and red boxes correspond to linear, 1.5, and quadratic mortality schemes, respectively

primary production arising from uncertainties in the functional form of non-predatory mortality were often obscured by other uncertainties in the food-web parameterization. We tested both the distributions of biomass and net production of each consumer to see whether they were significantly higher or lower under the linear mortality structure than with the quadratic structure. Even following the strongest perturbation, the majority of variables did not display any statistically significant differences (Mann-Whitney U-test, $\alpha = 0.05$) in their distributions. The exceptions to this fell into 2 groups. First, as with the relative metric discussed in the previous paragraph, functional groups with a high non-predatory mortality rate, including jellyfish, salmon, mammals, orcas, and gelatinous zooplankton, showed significantly higher biomass and production values under the linear mortality structure than the quadratic one. At the other end of the trophic spectrum, microzooplankton, copepod, and large zooplankton biomass were all lower under the linear scheme than the quadratic one (Fig. 7). This difference at the bottom of the food chain stems from changing predation pressure as a result of the amplified response of the primary predators of these organisms, particularly of the jellyfish group.

Table 2. Regression analysis of the relative amplification metric between quadratic and linear regimes revealed significant (all at $p < 0.001$) but low correlations with trophic level and ecotrophic efficiency. Regressions included 1050 observations (1 per consumer–ensemble pair)

Predictor	Coefficient of determination (R^2)	F
Trophic level	0.114	55.67
Ecotrophic efficiency	0.147	73.12
Both (no interaction)	0.183	63.74
Both (with interaction)	0.185	35.48

DISCUSSION

This analysis revealed a complex response to a seemingly straightforward perturbation, and also demonstrated the interplay of structural and parameter uncertainty in determining the range of simulated responses. First, this set of model simulations demonstrated that the interacting effects of light limitation, temperature dependence, and nutrient limitation on each individual phytoplankton group, as well as their indirect effects on each other through top-down effects of changing grazing pressure, can lead to unexpected changes in primary production even with a
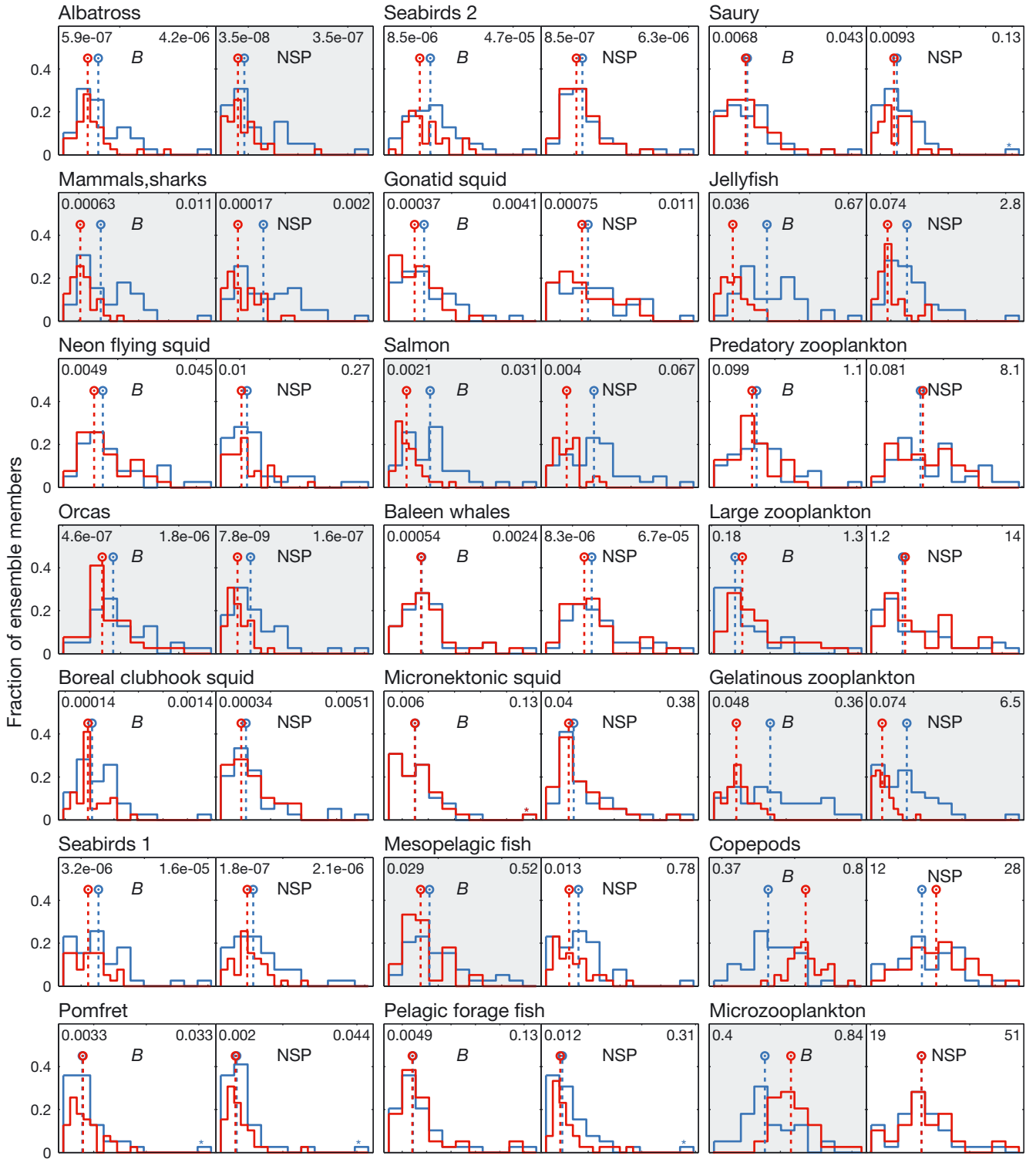
Fig. 7. Distributions of biomass (B, g C m^{-2}) and net secondary production (NSP, g C m^{-2} yr^{-1}) for each consumer in the food web under the linear (blue) and quadratic (red) mortality structures, at the end of the 5.0× surface iron flux perturbation. The median values of each dataset are indicated by the dotted stem lines. The shaded panels indicate variables where the median value is significantly higher or lower under the linear regime than the quadratic regime. All axes share the same vertical range, which indicates the fraction of ensemble members falling in a given range. Horizontal axis limits are labeled in the upper corners of each axis

relatively simple forcing factor. While both phytoplankton groups benefit directly—through an increased growth rate—from the increased iron deposition levels, increased annual net primary production was isolated to only one of these functional groups. Before running the simulations, we hypothesized that the large phytoplankton would be more likely to benefit from the increased iron levels, since the common assumption in plankton models is that small phytoplankton are more tightly regulated by the quick-responding microzooplankton (Armstrong 1999, Dunne et al. 2005). Although the small phytoplankton population was initially prevented from expanding due to microzooplantkon grazing, over time the microzooplankton population was reduced by a growing mesozooplankton community that also fed on large phytoplankton, releasing small phytoplankton from both predatory and competitive pressure.

Although our simulations, with their long-term changes in surface iron flux, cannot be directly compared with short-term iron fertilization experiments, it is interesting to note that iron addition experiments in the subarctic Pacific region have demonstrated mixed responses by the phytoplankton community. Since the iron hypothesis was first proposed as a mechanism for incomplete nutrient use in this region (Martin & Fitzwater 1988, Martin et al. 1989), 3 mesoscale iron fertilization experiments have been carried out in the Eastern Subarctic gyre: the Subarctic iron Enrichment for Ecosystem Dynamics Study (SEEDS) in 2001, Sub-arctic Ecosystem Response to Iron Enrichment Study (SERIES) in 2002, and SEEDS II in 2006. All 3 experiments were conducted during late summer, which is the approximate mid-point of the phytoplankton growing season in this region. The phytoplankton communities were very similar before fertilization for all 3 experiments, with the small phytoplankton (primarily prymnesiophytes and chlorophytes) dominating, and similar chlorophyll levels were measured each time (Suzuki et al. 2009). Over the 13 d post-fertilization observation period, SEEDS saw an increase of 2 to 5 times in the nanoplankton, but the response was dominated by a 45-fold increase in the diatom community, with a shift towards centric diatoms (Takeda & Tsuda 2005). The SERIES experiment observed increases in all size classes over the first 10 d of observations, followed by a bloom of diatoms, this time primarily the smaller pennate diatoms, over the final 8 d of observation (Marchetti et al. 2006). Contrary to these 2 studies, the SEEDS II fertilization observed no bloom of diatoms, with the picophytoplankton instead dominating the increase in biomass and productivity seen

over the 26 d study (Uematsu et al. 2009). The diversity of responses may indicate that higher predation closures are more dynamic than we consider them, and that they may induce structural changes in the planktonic food web.

In our study, the upper-trophic-level consumers showed fairly regular increases in production as a result of the increased primary production. Despite the complex network of pathways connecting the various functional groups to each other, there were no clear 'winners' or 'losers' resulting from this particular ecosystem perturbation. Instead, all consumer groups tended to experience an increase in both net production and biomass following 10 yr of increased primary production.

We found that when looking at an individual set of model parameters (i.e. one ensemble member), the structural form of non-predatory mortality could affect whether the increased production was amplified as it moved up the food chain. Linear mortality functions, which do not increase in prominence as a system becomes more productive, tend to pass large fractions of the increased production to the top of the food web, benefiting top predators more so than lower-trophic-level consumers. In contrast, quadratic mortality functions lead to damping of this response, as more of the increased production is recycled through the non-predatory loss terms rather than being passed to higher-trophic-level predators. The difference between these 2 structural regimes should be considered when constructing complex ecosystem models, particularly when not explicitly accounting for the uncertainty in input parameters. Often, ecosystem studies look only at the relative change in population variables, rather than the absolute change, recognizing that input uncertainty may render the absolute change less useful than the relative change. However, this study demonstrates that the relative change in ecosystem variables can be strongly influenced by structural uncertainties, more so than the absolute values of these variables.

However, whether choices regarding the functional form of non-predatory mortality significantly altered the range of predicted productivity of a single group varied based on other sources of uncertainty. When considering the full range of parameter uncertainty, we found that the differences in the responses predicted by the 3 non-predatory mortality structures could only be seen for a few variables, related to top predators with low predatory mortality. The salmon group (representing the most commercially important species in this food web), though, was one of the functional groups that did show different responses

under different mortality structures. Because we did not explicitly model fishing mortality, loss to fishing pressure was considered part of this functional group's non-predatory mortality. This perturbation experiment supports the importance of understanding the correct structural form of fishing loss and other non-predatory losses when modeling fisheries target groups.

In this context, our coupling of biogeochemistry to a food web has not completely eliminated closure terms, but rather pushed them higher in the food chain, towards the level of commercially targeted species and the fisheries that 'prey' on them. The likely role of fishing in these closure terms makes it essential to further push the end-to-end concept towards the links connecting the diverse social and economic factors that control dynamic fishing responses.

LITERATURE CITED

Armstrong R (1999) Stable model structures for representing biogeochemical diversity and size spectra in plankton communities. J Plankton Res 21:445–464

Aydin KY, McFarlane GA, King JR, Megrey BA, Myers KW (2005) Linking oceanic food webs to coastal production and growth rates of Pacific salmon (*Oncorhyncus* spp.), using models on three scales. Deep-Sea Res II 52:757–780

Aydin K, Gaichas S, Ortiz I, Kinzey D, Friday N (2007) A comparison of the Bering Sea, Gulf of Alaska, and Aleutian Islands large marine ecosystems through food web modeling. NOAA Tech Memo NMFS-AFSC-178

Boyd PW, Ellwood MJ (2010) The biogeochemical cycle of iron in the ocean. Nat Geosci 3:675–682

Brodeur R, McKinnell S, Nagasawa K, Pearcy W, Radchenko V, Takagi S (1999) Epipelagic nekton of the North Pacific subarctic and transition zones. Prog Oceanogr 43:365–397

Brussaard CPD (2004) Viral control of phytoplankton populations: a review. J Eukaryot Microbiol 51:125–138

Chassot E, Mélin F, Le Pape O, Gascuel D (2007) Bottom-up control regulates fisheries production at the scale of eco-regions in European seas. Mar Ecol Prog Ser 343:45–55

Christensen V, Pauly D (1992) ECOPATH II: a software for balancing steady-state ecosystem models and calculating network characteristics. Ecol Model 61:169–185

Christensen V, Walters CJ (2004) Ecopath with Ecosim: methods, capabilities and limitations. Ecol Model 172:109–139

Duggen S, Croot P, Schacht U, Hoffmann L (2007) Subduction zone volcanic ash can fertilize the surface ocean and stimulate phytoplankton growth: evidence from biogeochemical experiments and satellite data. Geophys Res Lett 34:L01612, doi:10.1029/2006GL027522

Dunne JP, Armstrong RA, Gnanadesikan A, Sarmiento JL (2005) Empirical and mechanistic models for particle export ratio. Global Biogeochem Cycles 19:GB4026, doi:10.1029/2004GB002390

Edwards AM, Yool A (2000) The role of higher predation in plankton population models. J Plankton Res 22:1085–1112

Fan SM (2008) Photochemical and biochemical controls on reactive oxygen and iron speciation in the pelagic surface ocean. Mar Chem 109:152–164

Flynn KJ (2005) Incorporating plankton respiration in models of aquatic ecosystem function. In: del Giorgio P, Williams P (eds) Respiration in aquatic ecosystems. Oxford University Press, Oxford, Chap 13

Frank KT, Petrie B, Shackell NL, Choi JS (2006) Reconciling differences in trophic control in mid-latitude marine ecosystems. Ecol Lett 9:1096–1105

Friedland KD, Stock C, Drinkwater KF, Link JS and others (2012) Pathways between primary production and fisheries yields of large marine ecosystems. PLoS ONE 7:e28945

Johnson KS, Gordon R, Coale KH (1997) What controls dissolved iron concentrations in the world ocean? Mar Chem 57:137–161

Kearney KA (2012) An analysis of marine ecosystem dynamics through development of a coupled physical-biogeo-chemical-fisheries food web model. PhD thesis, Princeton University

Kearney KA, Stock C, Aydin K, Sarmiento JL (2012) Coupling planktonic ecosystem and fisheries food web models for a pelagic ecosystem: description and validation for the subarctic Pacific. Ecol Model 237–238:43–62

Luo C, Mahowald N, Bond T, Chuang PY and others (2008) Combustion iron distribution and deposition. Global Biogeochem Cycles 22:GB1012, doi:10.1029/2007GB002964

Mahowald NM, Engelstaeder S, Luo C, Sealy A and others (2009) Atmospheric iron deposition: global distribution, variability, and human perturbations. Annu Rev Mar Sci 1:245–278

Marchetti A, Sherry ND, Kiyosawa H, Tsuda A, Harrison PJ (2006) Phytoplankton processes during a mesoscale iron enrichment in the NE subarctic Pacific. I. Biomass and assemblage. Deep-Sea Res II 53:2095–2113

Martin JH, Fitzwater SE (1988) Iron deficiency limits phytoplankton growth in the north-east Pacific subarctic. Nature 331:341–343

Martin JH, Gordon RM, Fitzwater S, Broenkow WW (1989) VERTEX: phytoplankton/iron studies in the Gulf of Alaska. Deep-Sea Res A 36:649–680

May R, McLean A (2007) Theoretical ecology: principles and applications, 3rd edn. Oxford University Press, Oxford

Moxim WJ, Fan SM, Levy H (2011) The meteorological nature of variable soluble iron transport and deposition within the North Atlantic Ocean basin. J Geophys Res 116:D03203, doi:10.1029/2010JD014709

Ohman MD, Hirche HJ (2001) Density-dependent mortality in an oceanic copepod population. Nature 412:638–641

Pauly D, Christensen V (1995) Primary production required to sustain global fisheries. Nature 374:255–257

Ryther JH (1969) Photosynthesis and fish production in the sea. Science 166:72–76

Steele JH, Henderson EW (1992) The role of predation in plankton models. J Plankton Res 14:157–172

Steinacher M, Joos F, Frolicher T, Bopp L and others (2010) Projected 21st century decrease in marine productivity: a multi-model analysis. Biogeosciences 7:979–1005

Stock CA, Dunne JP, John J (in press) Global-scale carbon and energy flows through the marine planktonic food web: an analysis with a coupled physical-biological model. Prog Oceanogr, doi: 10.1016/j.pocean.2013.007.001

Suzuki K, Saito H, Isada T, Hattori-Saito A and others (2009) Community structure and photosynthetic physiology of phytoplankton in the northwest subarctic Pacific during an *in situ* iron fertilization experiment (SEEDS-II). Deep-Sea Res II 56:2733–2744

Takeda S, Tsuda A (2005) An *in situ* iron-enrichment experiment in the western subarctic Pacific (SEEDS): introduction and summary. Prog Oceanogr 64:95–109

Thornton D (2002) Diatom aggregation in the sea: mechanisms and ecological implications. Eur J Phycol 37:149–161

Uematsu M, Wells ML, Tsuda A, Saito H (2009) Introduction to subarctic iron enrichment for ecosystem dynamics study II (SEEDS II). Deep-Sea Res II 56:2731–2732

Ware DM, Thomson RE, Thompson RE (2005) Bottom-up ecosystem trophic dynamics determine fish production in the Northeast Pacific. Science 308:1280–1284